Experimental and numerical characterizations of acoustic damping rates in a coupled-cavity configuration

Robin Nez, Manuel Gonzalez Flesca, David Marchal, Schmitt Thomas, Philippe Scouflaire, Sebastien Candel, Sebastien Ducruix

DOI:

Experimental and numerical characterizations of acoustic damping rates in a coupled-cavity configuration

R. Nez[1,2], *M. Gonzalez-Flesca*[1,2], *D. Marchal*[1], *T. Schmitt*[1], *P. Scouflaire*[1], *S. Candel*[1], *S. Ducruix*[1]
[1]*Laboratoire EM2C, CNRS, CentraleSupélec, Université Paris-Saclay - 3, rue Joliot-Curie, 91190 Gif-sur-Yvette, France*
[2]*CNES DLA - 52, rue Jacques Hillairet, 75612 Paris Cedex, France*
david.marchal@centralesupelec.fr
†Corresponding author : David Marchal

Abstract

This work aims at a better understanding of damping in coupled-cavities configurations such as liquid rocket engines (LRE). A cold flow rig called NPCC (New Pressurized Couple Cavities) is employed. It consists of two cavities mimicking dome and combustion chamber, linked by three injectors. The cavities can be either continuously excited or successively excited then relaxed by two different perforated rotating wheels placed at the outlets. Eigenmodes are first characterized. The rig is then excited at three successive eigenfrequencies using continuous modulation. The modes structures are checked using pressure transducers. Velocities at the injector's exits are measured with hot wires to characterize the injector's response. Forcing followed by relaxation (alternating forcing) is then used to study the damping rate of each mode, which is retrieved from the pressure transducers signal. 2D unsteady numerical simulations are performed to retrieve these values, both for continuous and alternating modulation. In the damping rate study, at least 10 excitation/relaxation cycles are necessary to achieve good convergence. The results are shown to be independant from the location of the probe used to derive the damping rate. The results are in reasonable agreement with the experiments for the three modes studied with continuous modulation. The study of the damping rate will however require 3D simulations to achieve good results with the methods presented here.

1. Introduction

Since the Apollo program in the 1960s, high-frequency combustion instabilities have been responsible for many delays in the access to space[1] . In liquid rocket engines, they are the result of the complex interaction between a turbulent flow, a confined chamber with its acoustic eigenmodes and the combustion that takes place in it. This interaction being not yet completely understood, engineers often rely on costly trial and error processes, with minor increments between two full scale tests. However, the increase of computing power in the recent years gives us an alternative to tackle the problem of combustion instabilities : by correctly simulating the system, one could get rid of the uncertainty behind the development of the next generation of rocket engines.
In particular, large eddy simulation (LES) has enlightened several mechanisms that take place in transcritical and supercritical cryogenic flames found in liquid rocket engines.[2–4] Injector dynamics, flame anchoring and flame-acoustic field interaction simulations help us understand the complex mechanisms leading to combustion instabilities.
Lab-scale experiments are crucial to validate these new codes : non-reacting test rigs,[5–7] simplified hot flow configurations[8,9] and even a reduced-scale rocket engine[10–12] have been designed in the past few years to study combustion instabilities, in parallel with their simulation.
With the help of theoretical works,[13] experiments and simulations have shown that fluctuations of chamber pressure as well as changes of the injection mass flow rate could lead to an unsteady release of the heat by flames. These are examples of source terms that drive combustion instabilities. They are in competition with damping terms, which will tend to decrease the amplitude of the pressure oscillations. This damping will be studied here, in a cold flow test rig developed by Méry et al.[14] and experimented by Gonzalez-Flesca et al.[15] This paper presents ongoing results obtained with unsteady simulations of this experiment.
First, Sec. 2 summarizes the theory and modelling of the acoustic damping rate. Sec. 3 presents the NPCC test rig used in the experiments. Then, Sec. 4 shows how this test rig is simulated in 2D using the AVBP software from CERFACS and IFPEN. The comparison between simulation and experimental results is displayed in Sec. 5, as well as

the post-processing methods used. Conclusion and perspectives are drawn in sec. 6.

2. Study of the acoustic damping rate

2.1 Theory and modelling

The study of the acoustic damping is made in the framework of reduced order modeling.[15] The state variables are projected on the eigenmodes of the system. The relaxation of an acoustic eigenmode m, in the absence of thermoacoustic source term and external forcing is given by :

$$\ddot{\eta}_m(t) + \omega_m^2 \eta_m(t) = -D_m(t) \tag{1}$$

where η_m is the amplitude of the mode, ω_m its angular frequency and D_m the damping term corresponding to that mode. Assuming linear damping, D_m is expressed as :

$$D_m(t) = 2\alpha_m \dot{\eta}_m(t) \tag{2}$$

where α_m is called the damping rate of mode m. The general solution of (1) is:

$$\eta_m(t) = e^{-\alpha_m t}(a \exp[it(\omega_m^2 - \alpha_m^2)^{1/2}] + b \exp[it(\omega_m^2 - \alpha_m^2)^{1/2}]) \tag{3}$$

where a and b are integration constants. The response of the system is therefore pseudo-harmonic, with a decaying envelope described by the factor $\mathrm{e}^{-\alpha_m t}$.
The object of this study is to determine α_m, in both the experiment and the simulation. Two methods described below are used in the experiments : the alternating forcing method and the Full Width at Half Maximum (FHWM) method. Only the alternating forcing method is used in the simulations.

2.2 Alternating forcing method

In order to study the damping rate of the acoustic modes, the NPCC test bed described in Sec.3 will undergo acoustic modulation followed by relaxation. The forcing is applied using a half-perforated wheel described below. During the relaxation, there is no more external forcing which corresponds to the framework of Eq. (1).
This modulation will be referred to as 'alternating forcing' in the following.

2.3 FWHM method

Another way to determine α is to perform a continuous modulation by exciting the NPCC test bench with a fully perforated wheel described in Sec.3 and progressively increase the rotation speed of the wheel. This method uses the result of Siebert[16] :

$$\alpha = \pi \Delta f \tag{4}$$

where α is the damping rate and Δf the Full Width at Half Maximum (FWHM), i.e. the width of the power spectrum of the pressure signal taken at half the peak amplitude. This method was applied by Webster et al.[17] in their analysis of the BKH model combustor. This method will not be used in the following study.

3. The NPCC test rig

In a typical liquid rocket engine, the propellants are conveyed through domes to the coaxial injectors: the oxidizer circulates through the central part of the injector, whereas the fuel comes through the annular part. Therefore, the possible coupling between the combustion chamber and the injection system can be the root cause of many combustion instabilities problems. The New Pressurized Coupled Cavities (NPCC) test rig is a cold flow experiment which allow intensive study of this coupling in a simplified configuration.

3.1 Configuration

The NPCC test rig is presented in Fig.1. It is made of aluminium and stainless steel rectangular cavities and mounted on a rail. From left to right : the first cavity is the dome fed by compressed air (3.5 bar) at ambient temperature. The following plate contains the three injectors, all with a 6mm diameter. The chamber is made of three parts. Parts 1 and 3 are fixed, whereas part 2 is interchangeable, adding the possibility to change the length of the chamber. At the end of the chamber, another plate contains two exit nozzles. These nozzles can be obturated with a partially perforated wheel driven by an electric motor, this setup is called the Very High Amplitude Modulator (VHAM).[6]

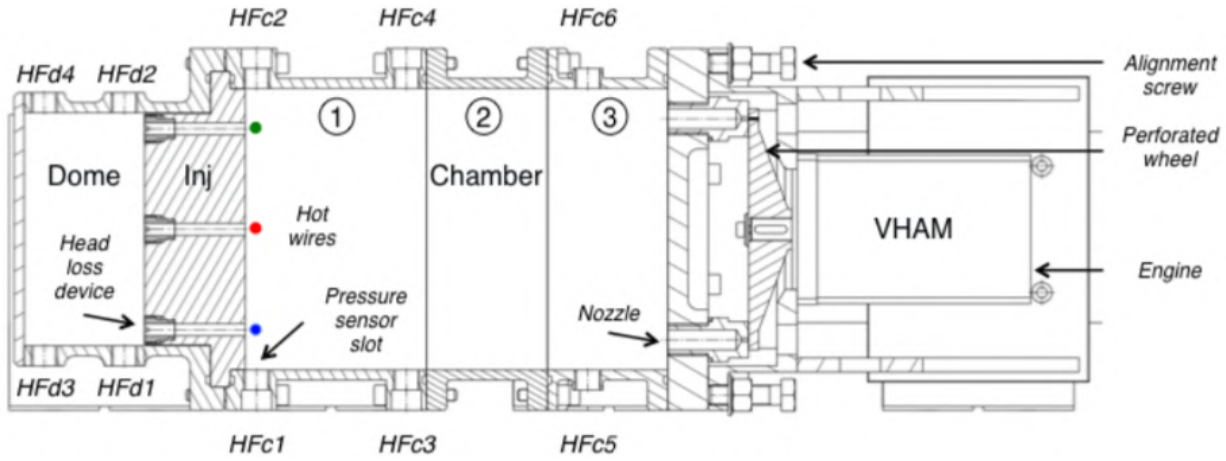

Figure 1: NPCC test rig

The electric motor has a maximum rotation speed of 6000 rpm. The program controlling the engine has two modes: it can run at a constant speed or progressively increase in speed, doing a ramp. Fig. 2 presents the two different perforated wheels that have been designed: one fully perforated to constantly excite the system, one partially perforated to alternate between excitation and relaxation. With 69 perforations on the standard wheel, the maximum modulation frequency is 6900 Hz.

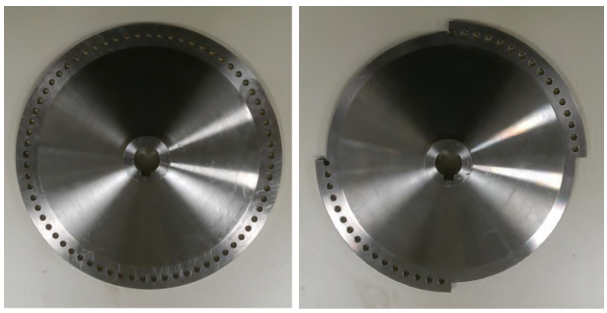

Figure 2: Fully perforated wheel (left), partially perforated wheel (right)

The test rig is equipped with probes for pressure measurements: 4 in the dome (Hfd*n* in Fig.1) and 6 in the chamber (HFc*n* in Fig.1). Their positions are chosen to clearly identify the acoustic modes studied (Sec 3.2). Hot wire sensors (calibrated before performing any experiment) are used at the end of the injectors to measure the injection velocities. The operating pressure is 3.5 bar. The air stream is controlled by a mass flow meter.

The compressed air in the dome flows through the injectors to the chamber, where the internal pressure is modulated by the VHAM. The perforated wheel is alternatively obturating each nozzle, maintaining a constant escaping flow rate and thus a constant pressure in the chamber. This modulation creates acoustic waves inside the system, leading to the installation of acoustic standing modes, whose shapes depend on the frequencies of excitation.

3.2 Eigenmodes and eigenfrequencies

The eigenmodes of the system define the resonant frequencies at which the system will respond with the highest intensity. The ramp mode of the motor is well-suited for recovering these frequencies: the frequency of modulation is slowly increased from 0 Hz to 3000 Hz during a ramp of 99s. The pressure signal recovered at HFc1 and HFd1 is

shown in Fig. 3a. A time-frequency analysis (Fig. 3b) provides the eigenfrequencies of the system by associating the times of maximum response with the modulation frequency.

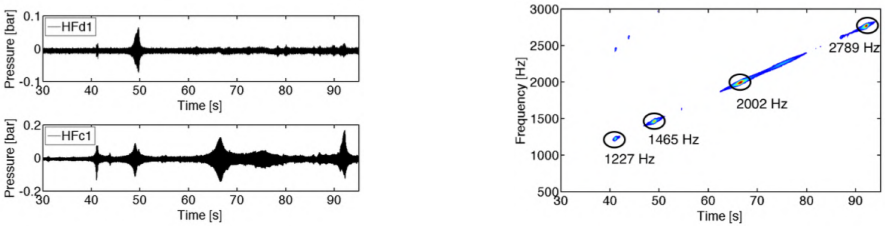

(a) (b)

Figure 3: (a) Pressure signal recorded at HFc1 (chamber) and HFd1 (dome) as a function of time during a ramp test, each peak corresponds to an eigenmode in the cavity. (b) Short time Fourier transform analysis of the signal detected by HFc1.

The AVSP Helmholtz solver[18] is used to check the eigenfrequencies with a simplified geometry (no nozzles). Results are close to those obtained using the ramp mode of operation (Table 1). Three eigenmodes will be studied in the present work: 1T, 1T1L and 1T2L. The 1T mode is fully transverse, while the 1T2L mode shows 2 pressure nodes along its longitudinal axis. The inner dimensions of the dome and chamber were chosen to match the first transverse eigenmode frequency of the dome ($1T^d$) with the first transverse first longitudinal mode of the chamber ($1T1L^c$). The 1T1L mode of the chamber is thus a coupled mode.

Table 1: Eigenfrequencies obtained from AVSP and the experiment

	1T	**1T1L**	**1T2L**
Calculated frequency, Hz	1210	1450	2009
NPCC measured frequency, Hz	1227	1465	2002

Fig. 4 presents the shape of these three modes, as found by AVSP. The simulations clearly confirm that the 1T1L mode of the chamber is coupled with the 1T mode of the dome, while the 1T and 1T2L modes of the chamber are not coupled with the dome.

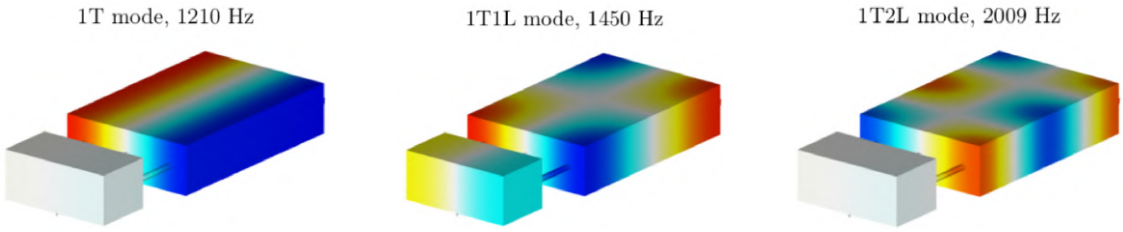

Figure 4: The selected set of eigenmodes found by the AVSP solver

4. 2D Numerical simulations

By considering a longitudinal cut through the plane containing the injectors, a 2D domain simplifying the experiment was created. This will not strictly account for the physics of the three dimensional problem, but allows for fast calculations and testing of the methodology which will be used later on the much more costly 3D simulations.

4.1 Governing equations, models and numerics

The Favre-filtered, fully compressible Navier-Stokes equations are used to formulate the Large Eddy Simulation (LES) approach. The fluid is air, its viscosity is calculated with the Sutherland method. The sub-grid scale stress tensor is modeled with the dynamic Smagorinsky model.[19] The SGS energy and species fluxes are modeled using the gradient transport assumption, introducing turbulent Prandtl and Schmidt numbers, both set to 0.6. Thermodynamics are modeled by the perfect gas equation.
The compressible unstuctured solver AVBP,[20,21] developed by CERFACS and IFPEN, is used. The numerical scheme is a third order in time and space Taylor-Galerkin scheme,[22] called TTGC.

4.2 Computational domain, mesh and boundary conditions

The computational domain is shown in Fig.5. It reproduces an axial cut of the geometry of the experimental setup. The dome is 60x110 mm, the chamber is 210x140 mm, the injectors are 6 mm in diameter and 50 mm long. The nozzles at the outlet are a bit different than the ones in the test rig. They were designed this way to better absorb the vortices that appear in the 2D simulation and to optimize the pressure modulation amplitude at the outlet without encountering any backflow. The inlet boundary is on the left side of the dome, contrary to the experiment where it is located on the upper side.
The 2D mesh contains 128000 nodes and 253000 cells. The smallest cells are located in the injectors, which contain 20 cells in their diameter (6 mm wide, cell size: 0.30 mm).
The inlet boundary condition is fully reflective for all frequencies. All solid boundary conditions are modeled with an adiabatic wall law.[23] A relaxation method on the pressure is used at the outlet, where superimposed ingoing sine acoustic waves are used to model the fully perforated wheel.

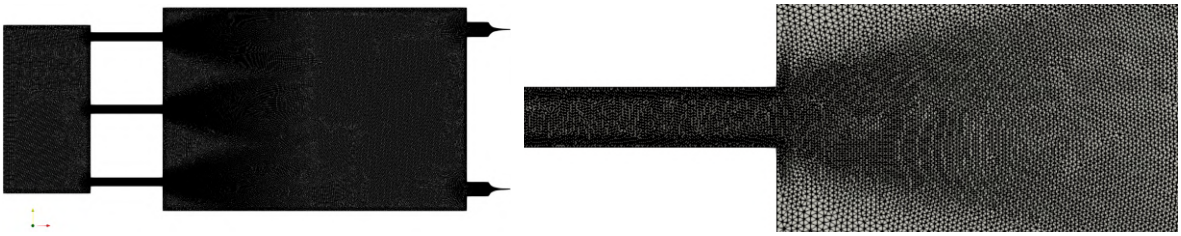

Figure 5: Left: Sketch of the mesh. Right: Zoom on one injector

4.3 Operating conditions

In this 2D simulation, bulk velocities in the injectors (u_{inj}) are conserved with respect to the experiment. The corresponding inlet velocity u_{inlet} is enforced on the left boundary of the dome which serves as the inlet here, due to the impossibility to reproduce the lateral feeding pipe in this plane. The mean chamber pressure p_c is maintained at 3.5 bar by enforcing a mean static pressure p_{out} = 2.95 bar at the outlet boundaries (isentropic expansion to Mach 0.45). The amplitude of the modulation is imposed at 0.4 bar.
The three eigenmodes studied by Gonzalez-Flesca et al.[15] are simulated by imposing alternatively pulsed boundary conditions at the outlet. The operating conditions are summarized in Table 2.

Table 2: Operating conditions of the 2D simulation

p_c	3.5 bar
u_{inj}	17.6 m.s^{-1}
u_{inlet}	1.37 m.s^{-1}
ρ^0_{inlet}	4.1 kg.m^{-3}
T^0_{inlet}	293 K
p_{out}	2.95 bar

4.4 Implementation of the alternating forcing

To reproduce the alternating forcing method used for the damping rate study in the simulation, sine ingoing acoustic waves at the outlet boundaries are modulated with a square function, equal to 1 during the excitation and 0 during the relaxation.
It was observed that the signals gathered from the experiment at the HFc1 probe did not reach the limit cycle after one excitation cycle (corresponding to the rotation of the part containing 16 holes in the perforated part of the wheel).[15] Therefore, it was decided to increase the duration of the excitation-relaxation cycle to 64 periods in the simulations: 32 for the excitation, 32 for the relaxation. Fig. 6 illustrates this choice by showing a few cycles as measured by a probe located at the bottom nozzle's end (where the boundary condition is applied), during a 1T excitation-relaxation calculation.
The operating conditions are the same as in the continuous modulation case (Table 2).

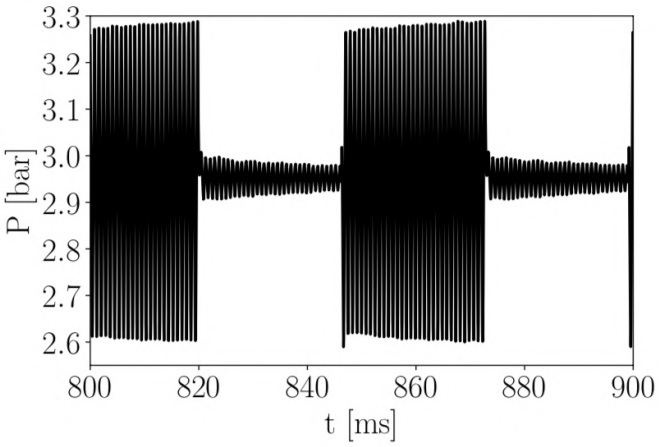

Figure 6: Signal measured at the outlet boundary (bottom nozzle) for the 1T alternating forcing method. 32 periods of modulation are followed by a time of relaxation corresponding to the 32 periods again.

5. Results, comparisons between simulation and experiment

5.1 Continuous modulation

In this section, simulations are performed using a continuous modulation at a frequency that successively corresponds to the 3 modes presented. In particular, the shape of the modes, the injector velocity evolution and the acoustic pressure amplitudes are compared to the experiments.

Fig. 7 presents instantaneous fields of acoustic pressure. Qualitative comparisons with Fig. 3 show that the mode structures are well retrieved by the simulations. The coupling between cavities of the 1T1L mode is clearly visible.

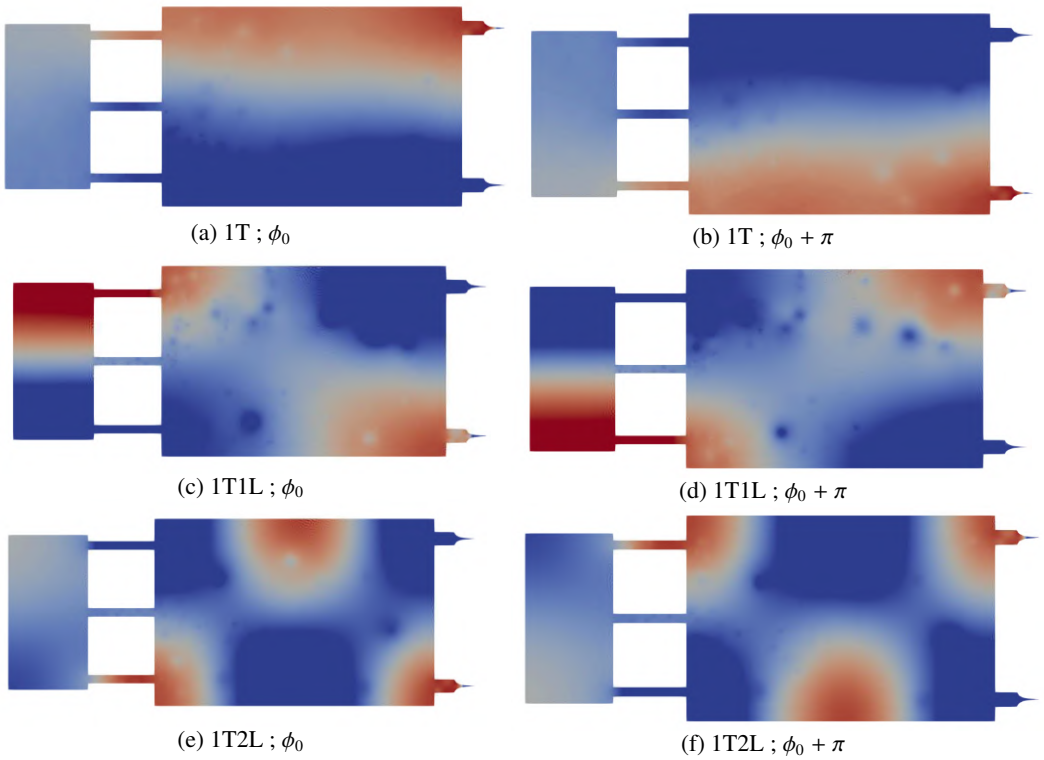

(a) 1T ; ϕ_0 (b) 1T ; $\phi_0 + \pi$

(c) 1T1L ; ϕ_0 (d) 1T1L ; $\phi_0 + \pi$

(e) 1T2L ; ϕ_0 (f) 1T2L ; $\phi_0 + \pi$

Figure 7: Instantaneous pressure fields for cases 1T, 1T1L and 1T2L given at two instants in phase opposition. Red: maximum, Blue: minimum

Fig. 8 presents velocity fluctuations as measured experimentally by the hot wires HW1, HW2 and HW3 (see Fig. 1 for the probe positions). Both experimental and numerical signals have been filtered with a 3rd order Butterworth bandpass filter, with high and low cut-off frequencies at 200 Hz above and below the modulation frequency for each case.[24]
The velocity fluctuations for cases 1T1L and 1T2L are qualitativelty well-recovered, amplitudes being properly reproduced. Case 1T shows large discrepancies with the experimental measurements, both in terms of phase between the signals and amplitude. This question is still under investigation.

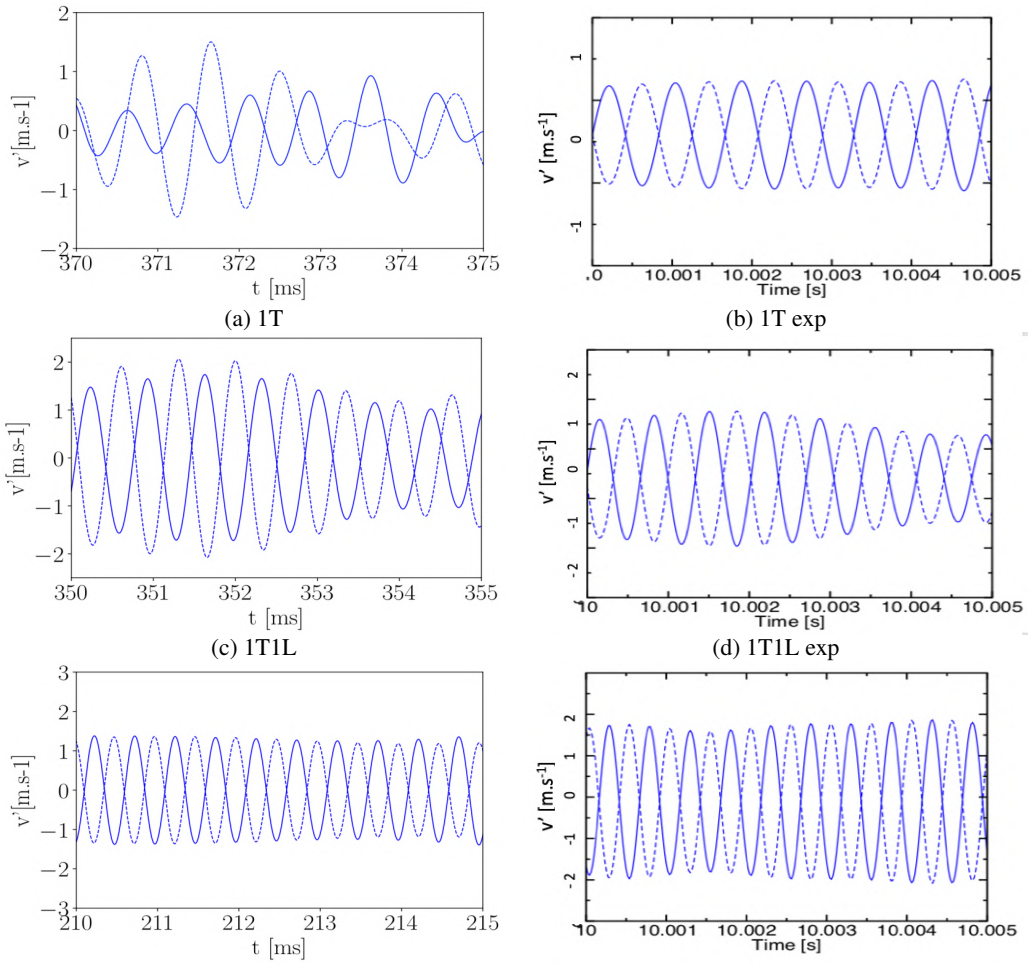

(a) 1T (b) 1T exp
(c) 1T1L (d) 1T1L exp
(e) 1T2L (f) 1T2L exp

Figure 8: Injector axial velocity component given by the 2D simulation (left) and the experiment (right). – Signal for HW1 – – Signal for HW3

Fig. 9 presents the pressure signals measured by the HFc1 (chamber) and HFd1 (dome) probes (see Fig. 1 for the probe positioning). The signals from the simulation have been filtered to remove the mean value, using a high pass filter with a cut-off frequency of 10% of the modulation frequency.
Considering the 1T mode, the amplitude in the chamber is well-retrieved for HFc1 in the simulation but the HFd1 signal has a higher amplitude than in the experiment. For the excitation of the 1T1L coupled mode both signals are in phase with what was expected (see figs. 3 and 5). The amplitude in the dome is well-retrieved, but the chamber amplitude is lower than in the experiment. The 1T2L mode is again the one that is reproduced the best by the simulation.

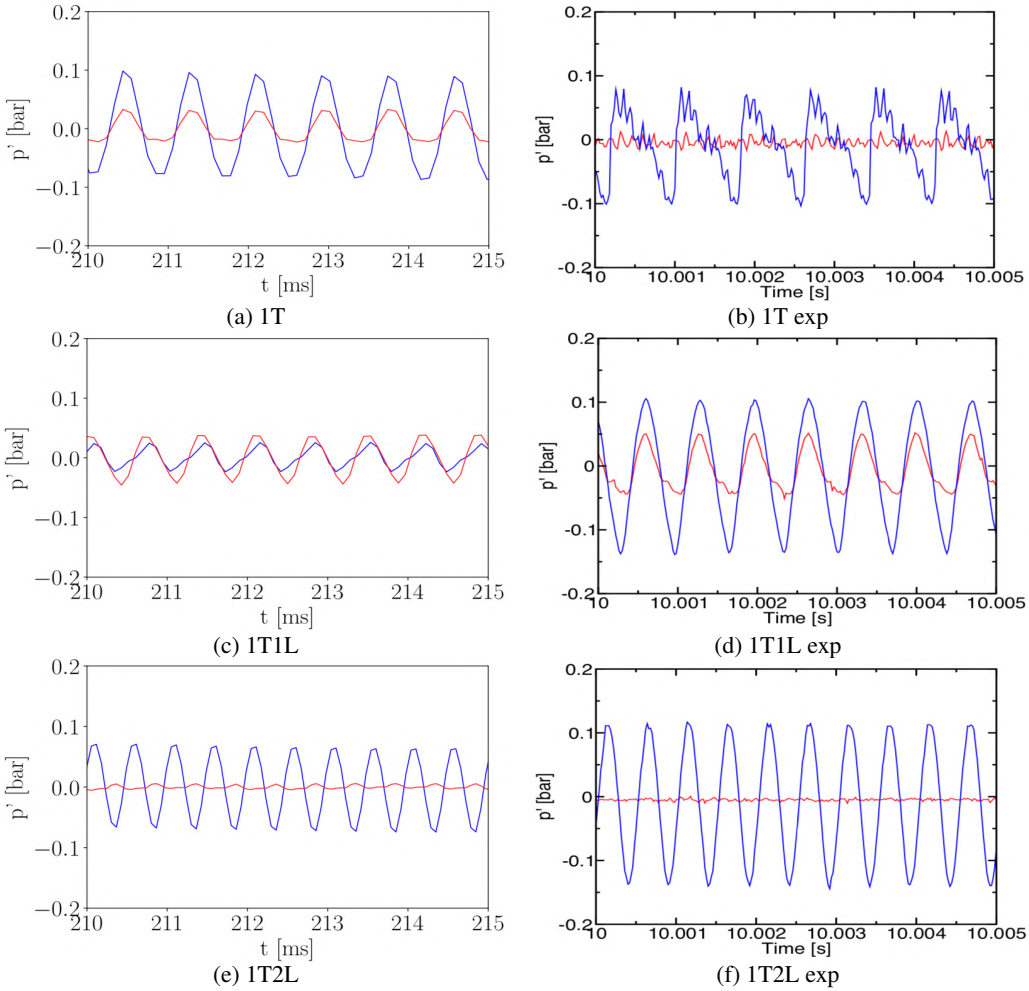

Figure 9: Pressure signals recorded by HFc1 (blue) and HFd1 (red) probes. On the left, 2D simulations. On the right, experiments.

5.2 Study of the damping rate

In this section, the alternating forcing method is used on the NPCC test rig, as described in Sec. 3 for the experiments and Sec. 4 for the simulations.

5.2.1 Post-processing methods

The pressure signal is recovered from the probes, treated with a Hilbert transform to extract its envelope. Two sub-methods are then used : each decaying slope can be fitted with an exponential function to measure its damping rate and a statistical average of each damping rate value can be performed (**statistical method**), or the average cycle can be computed using phase locking and the exponential fitting can be made on its envelope (**average cycle method**). Only the statistical method was performed by Gonzalez-Flesca et al. to treat the results extracted from the experiments, whereas both methods are used here for the simulation results.
Fig. 10 gives an overview of the methods applied on the 1T simulated case.

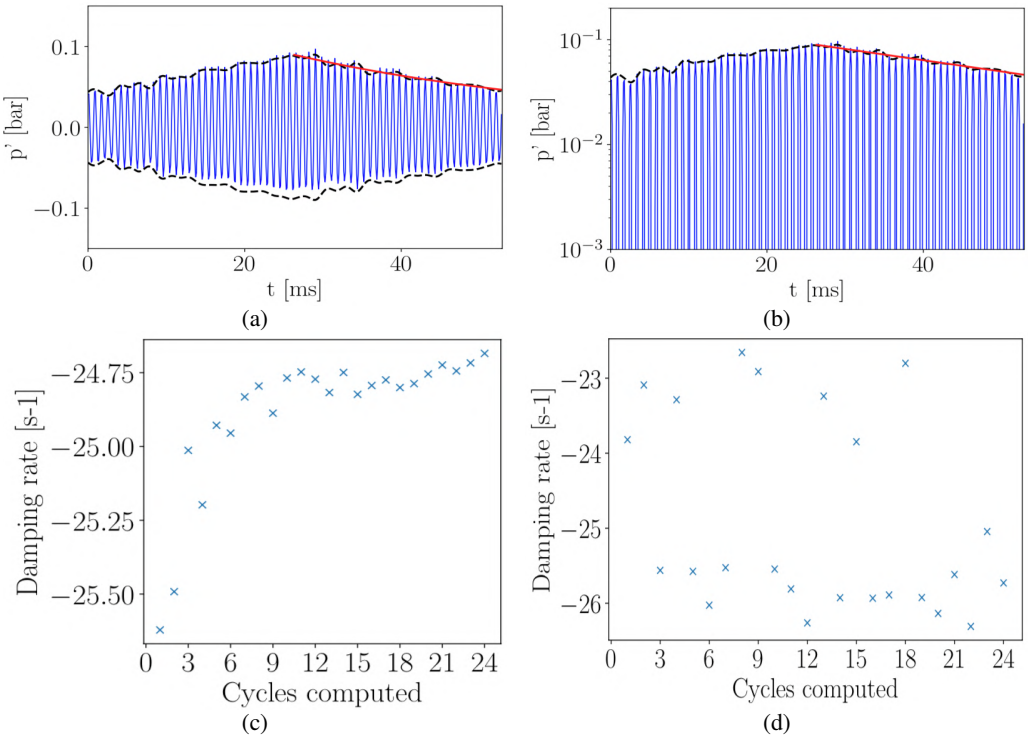

Figure 10: Damping rate determination for the 1T simulated mode, using the pressure signal from HFc1 probe. (a) Average cycle of the pressure signal (–), envelope (– –), exponential fit (–) (b) Logarithm of the average cycle (c) Damping rate determined by the average cycle method with respect to the number of cycles computed (d) Damping rate evaluated for each cycle and used by the statistical method with respect to the number of cycles computed

5.2.2 Convergence of the damping rate

It was observed that at least 10 cycles were needed in order to have a good convergence of the damping rate for the cases 1T and 1T1L and even more for the case 1T2L. This is not an issue for the 2D simulations but could be problematic if this methodology is applied to more expensive 3D simulations. Fig. 11 illustrates this by showing the damping rates obtained with the average cycle method with respect to the number of cycles computed.

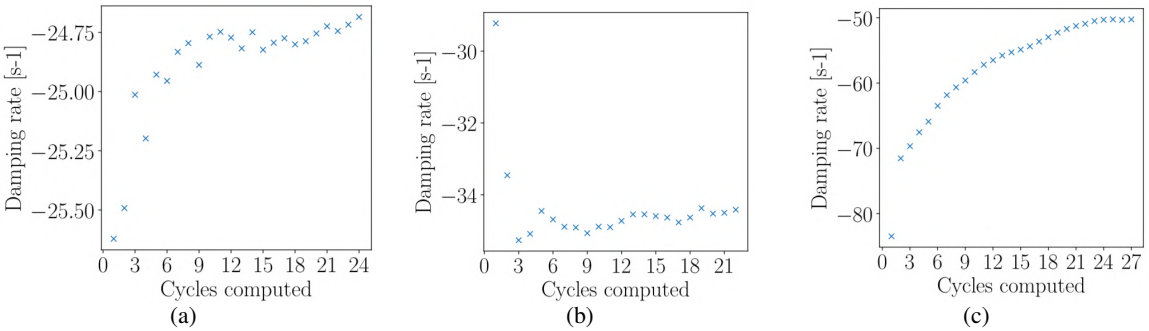

Figure 11: Damping rates obtained by the average cycle method. (a) 1T mode (b) 1T1L mode (c) 1T2L mode

5.2.3 Comparison between experiment and simulations for the damping rate evaluation

The results of the damping rate study are presented in Table 3. Experimental results are reproduced from Gonzalez-Flesca et al.[24]

Table 3: Damping rate results

			1T	**1T1L**	**1T2L**
Experimental	Statistical method	Damping rate [s^{-1}]	36	85	61
		N - σ[%]	30 - 4	30 - 3	30 - 4
Simulation	Statistical method	Damping rate [s^{-1}]	25	33	50
		N - σ[%]	24 - 4	23 - 10	27 - 7
	Average cycle method	Damping rate [s^{-1}]	25	34	50

N is the number of cycles used to determine the damping rate in the statistical method, σ is the relative standard deviation in percentage.

The experiments on the NPCC test rig using alternating forcing by Gonzalez-Flesca et al. led to series of 30 cycles for each excited mode, which were then treated using the statistical method.
Simulations are performed for more than 20 cycles for each mode, which gives a relevant amount of statistical points. The damping rates retrieved are lower than the experimental ones for modes 1T and 1T2L and much lower for mode 1T1L. This is probably due to two-dimensional effects. A 3D simulation using the methodology described here is therefore needed.

5.2.4 Influence of the probe position

A study was conducted on the 1T mode to see whether the position of the probe had an influence on the evaluation of the damping rate. All signals from the 6 probes located in the chamber (HFcx) were studied with the average-cycle method and the statistical method presented earlier. The results are shown in Fig. 12. The damping rate value was found to be very close for each probe, with a maximum variation of 8% (2% if we consider only the average-cycle method). Therefore, the choice to study the signal from only one probe (HFc1) can be validated *a posteriori*.

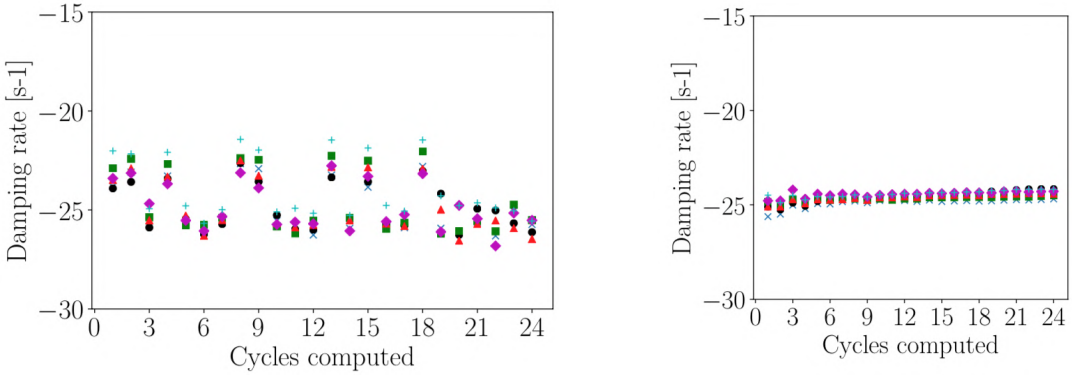

Figure 12: Dispersion with probe location of the damping rate using a) the statistical method and b) the average-cycle method. x HFc1, •$HFc2$, □$HFc3$, △$HFc4$, ⋄$HFc5$, +$HFc6$

6. Conclusion and perspectives

2D simulations of the NPCC test rig were presented in this paper. The objective is to study the response of a coupled cavity to modal excitation. The mode shape was recovered for the three modes studied experimentally. The results were in reasonable agreement in terms of injection velocity oscillations and acoustic pressure oscillations. Study of the damping rate led to the conclusion that at least 10 cycles were needed in order to obtain a good convergence of the results. Moreover, the damping rate was found to be independant of the position of the probe in the experiment. However, the damping rates found in the simulation were not comparable to the experimental ones, especially for the coupled mode 1T1L, despite good convergence. This is certainly due to the fact that simulations were two-dimensional. Current work focuses on the 3D simulation of the experiment, which will hopefully give better results using the methodology described here.

Acknowledgements

Support provided by ArianeGroup, the prime contractor of the Ariane launcher cryogenic propulsion system and CNES, the French National Space Agency, is gratefully acknowledged. This work was granted access to the HPC resources of IDRIS and CINES made available by GENCI (Grand Equipement National de Calcul Intensif) under the allocation A0042B06176. A part of this work was performed using HPC resources from the mesocentre computing center of Ecole CentraleSupélec and Ecole Normale Supérieure Paris-Saclay supported by CNRS and Région Ile-de-France.

References

[1] J. Oefelein and V. Yang, "Comprehensive review of liquid-propellant combustion instabilities in F-l engines," *Journal of Propulsion and Power*, vol. 9, Sept-Oct 1993.

[2] L. Hakim, T. Schmitt, S. Ducruix, and S. Candel, "Dynamics of a transcritical coaxial flame under high-frequency transverse acoustic forcing: The effect of a modulation frequency," *Combustion and Flame*, vol. 162, no. 10, 2015.

[3] J. Oefelein, "Thermophysical characteristics of shear-coaxial LOx-H2 flames at supercritical pressure," *Proceedings of the Combustion Institute*, vol. 30, no. 02, 2005.

[4] A. Urbano, Q. Douasbin, L. Selle, G. Staffelbach, B. Cuenot, T. Schmitt, S. Ducruix, and S. Candel, "Study of flame response to transverse acoustic modes from the LES of a 42-injector rocket engine," in *Proceedings of the Combustion Institute*, vol. 36, 2016.

[5] F. Richecoeur, *Experimentations et simulations numeriques des interactions entre modes acoustiques transverses et flammes cryotechniques*. PhD thesis, Ecole Centrale Paris, 2006.

[6] Y. Méry, *Mecanismes d'instabilites de combustion haute-frequence et application aux moteurs-fusees*. PhD thesis, Ecole Centrale Paris, 2010.

[7] L. Hakim, *Dynamics of Transcritical Coaxial Flames in High- Frequency Transverse Acoustic Fields: Application to Liquid Rocket Engine Instabilities*. PhD thesis, Ecole Centrale Paris, 2013.

[8] L. Vingert, M. Habiballah, P. Vuillermoz, and S. Zurbach, "MASCOTTE, a test facility for cryogenic combustion research at high pressure," in *51st International Astronautical Congress*, 2000.

[9] F. Richecoeur, P. Scouflaire, S. Ducruix, and S. Candel, "High-frequency transverse acoustic coupling in a multiple-injector cryogenic combustor," *Journal of Propulsion and Power*, vol. 22, no. 4, pp. 790–799, 2006.

[10] S. Groning, D. Suslov, J. S. Hardi, and M. Oschwald, "Influence of hydrogen temperature on the acoustics of a rocket engine combustion chamber operated with LOx/H2 at representative conditions," in *Proceedings of Space Propulsion*, 2014.

[11] S. Groning, D. Suslov, J. S. Hardi, and M. Oschwald, "Influence of hydrogen temperature on the stability of a rocket engine combustor operated with hydrogen and oxygen," *CEAS Space Journal*, 2016.

[12] T. Schmitt, G. Staffelbach, S. Ducruix, S. Groning, J. Hardi, and M. Oschwald, "Large-eddy simulations of a sub-scale liquid rocket combustor: influence of fuel injection temperature on thermo-acoustic stability," in *7TH EUROPEAN CONFERENCE FOR AERONAUTICS AND AEROSPACE SCIENCES (EUCASS)*, 2017.

[13] Y. Méry, "Impact of heat release global fluctuations and flame motion on transverse acoustic wave stability," in *Proceedings of the Combustion Institute*, 2017.

[14] Y. Mery, S. Ducruix, P. Scouflaire, and S. Candel, "Injection coupling with high amplitude transverse modes: experimentation and simulation," *Comptes Rendus Mécaniques*, vol. 337, no. 6-7, pp. 426–437, 2009.

[15] M. Gonzalez-Flesca, P. Scouflaire, T. Schmitt, S. Ducruix, and S. Candel, "Reduced order modeling approach to combustion instabilities of liquid rocket engines," *AIAA JOURNAL*, vol. 56, no. 12, pp. 1–13, 2018.

[16] W. M. Siebert, *Circuits, signals, and systems*, vol. 2, p. 63. MIT press, 1986.

[17] S. C. L. Webster, *Analysis of pressure dynamics, forced excitation and damping in a high pressure LOX/H2 combustor*. PhD thesis, Deutsches Zentrum fur Luft- und Raumfahrt, 2017.

[18] F. Nicoud, L. Benoît, and C. Sensiau, "Acoustic modes in combustors with complex impedances and multidimensional active flames," *AIAA Journal*, vol. 45, no. 426-441, 2007.

[19] M. Germano, U. Piomelli, P. Moin, and W. H. Cabot, "A dynamic subgridscale eddy viscosity model," *Phys. Fluids A*, vol. 3, no. 7, p. 1760, 1991.

[20] T. Schonfeld and M. Rudgyard, "Steady and unsteady flows simulations using the hybrid flow solver avbp," *AIAA Journal*, vol. 37, no. 11, pp. 1378–1385, 1999.

[21] V. Moureau, G. Lartigue, Y. Sommerer, C. Angelberger, O. Colin, and T. Poinsot, "High-order methods for DNS and LES of compressible multi-component reacting flows on fixed and moving grids," *J. of Comput. Phys.*, vol. 202, no. 2, pp. 710–736, 2005.

[22] O. Colin and M. Rudgyard, "Development of high-order Taylor-Galerkin schemes for unsteady calculations," *J. Comput. Phys.*, vol. 162, no. 2, pp. 338–371, 2000.

[23] P. Schmitt, *Simulation aux grandes échelles de la combustion étagée dans les turbines à gaz et son interaction stabilité - polluants-thermique*. PhD thesis, INP Toulouse, 2005.

[24] M. Gonzalez-Flesca, *Simulation, experimentation and modeling contributions to the analysis of high frequency combustion instabilities in liquid propellant rocket engines*. PhD thesis, Université Paris-Saclay, CentraleSupélec, 2016.